ORIGINAL PAPER

Analysis of the first four moderate geomagnetic storms of the year 2015

Emre Eroglu[1]

Abstract

This essay investigates the first four *moderate* geomagnetic activities (the 04 January storm, the 07 January storm, the 17 February storm, and the 24 February storm) of 2015 in the 24th solar cycle. The essay attempts to understand these storms with the aid of zonal geomagnetic indices. It predicts the *zonal geomagnetic indices* (Dst, ap, AE) of the storms by an *artificial neural network model*. The phenomena that occurred in January and February are discussed by taking into account the *solar wind parameters* (B_z, E, P, N, v, T) and the zonal geomagnetic indices obtained from NASA. In the study, after glancing at the general appearance of the year 2015, which is exhibited with too small errors, binary correlations of the variables are indicated by the covariance matrix and the hierarchical cluster of the variables is presented by at dendrogram. The artificial neural network model is governed by the physical principles in the paper. The model uses the solar wind parameters as *inputs* and the zonal geomagnetic indices as *outputs*. The causality principle forms the models by cause–effect association. The back propagation algorithm is specified as Levenberg–Marquardt (trainlm), and 35 neural numbers are utilized in the artificial neural network. The neural network model predicts the Dst, ap, and AE indices of January and February geomagnetic storms with an accuracy that deserves discussion. The R correlation coefficients of the Dst, ap, and AE indices reach up to 98.9%. In addition to reliable accuracy, the parameters affecting the R correlation coefficients agree with the literature. Estimating the geomagnetic activities may support interplanetary works.

Keywords Solar wind parameters (SWp) · Zonal geomagnetic indices (ZGi) · Artificial neural network (ANN)

Introduction

Natural events are interpreted by mathematicians via data. Data are converted to variables, which later provide modeling opportunities to researchers. Depending on physical conditions, variables may be separated into dependent and independent ones. When the *solar wind parameters* (SWp) are considered to be independent variables, the *zonal geomagnetic indices* (ZGi) are considered to be dependent variables. Geomagnetic activities (Akasofu 1964; Kamide et al. 1998; Rathore et al. 2014) are also such natural events. This paper tries to understand and interpret the 04 January storm (Dst = − 71 nT), the 07 January storm (Dst = − 99 nT), the

17 February storm (Dst = − 64 nT), and the 24 February storm (Dst = − 56 nT) *moderate* geomagnetic activities built on the SWp and the ZGi based on the cause (B_z, E, P, N, v, T)–effect (Dst, ap, AE) association. The storms are examined by an *artificial neural network* model (ANNm). In the ANNm, Levenberg–Marquardt (trainlm) is selected as the backpropagation (Rumelhart et al., 1986; Conway 1998) algorithm, and thirty-five neural numbers are utilized (Williams and Zipser 1989; Elman 1990; Gardner and Dorling 1998; Fausett 1994).

The sun is a plasma-dense energy and power source that produces durable magnetic waves. These magnetic waves are conveyed out to the interplanetary medium by the SWs. The SW has dense particles induced by the energy spreading from the sun (Parker 1958). Being swallowed by *coronal mass ejection* (CME) cloud of the earth's magnetosphere-ionosphere and the B magnetic field's B_z component orienting from the positive northward to the negative southward are invaluable for the geomagnetic storm. Shortly, the fast alteration in the magnetosphere of the earth governed by

✉ Emre Eroglu
eroglumre@gmail.com

[1] 1Department of Mathematics, Kirklareli University, Kirklareli 39100, Turkey

the SW scattering out of the sun is named a geomagnetic storm. CME is the burst of magnetically charged plasma into the interplanetary medium with high speeds. The dense magnetic field is burst in the solar corona (Lin and Ni 2018) by direct CMEs in a loop through (magnetic) reconnections (Kamide et al. 1998; Gonzalez et al. 1989; Borovsky 2012; Fu et al. 2013; 2017). Polarized magnetosonic waves and CME straightly turn out the SWp (Gonzalez et al. 1999). One of the governors' SWp is the magnetic field B_z component. The negative B_z magnetic field replaces from the northward to the southward. This orientation and decreasing cause of the terrestrial magnetic field by causing disturbances with magnetic reconnections. Turbulences and fluctuations in the magnetic field controlled by the storm disturbance storm time (Dst) index (Dungey. 1961; Sugiura. 1964) from ZGi can be called storms after the minimum peak B_z. The course of the storm has three phases: the *initial phase* (sudden commencement), the *main phase*, and the *recovery phase*. In the initial phase, in which the storm begins, the Dst index decreases from positive values to negative values supporting the magnetic field. In the main phase, the Dst index indicates negative values. After the negative values show the minimum values, the recovery phase begins. Lastly, the geomagnetic storm finishes with the recovery phase when the fluctuation in the magnetic field ends and the Dst index indicates the initial values. In moderate storms, following the B_z parameter of the Dst index with a delay (Burton 1975) of 5–6 h is the response of the ring current to the SW. To better understand a geomagnetic storm (Mayaud 1980; Eroglu 2018; Eroglu 2019; Inyurt and Sekertekin 2019; Inyurt 2020; Koklu 2020; Eroglu 2020), the author considers the models between the SWp and the ZGi. This paper utilizes hourly versions of the SWp and the ZGi.

This essay tries to investigate 04 January, 07 January, 17 February, and 24 February (2015) storms based on their physical requirements via an ANN model by meticulously governing the causality principle (Eroglu 2011, 2021; Eroglu et al. 2012a; 2012b). The ANN is a precious method; it may be utilized as an operative approach for estimation in scientific disciplines (Elman 1990; Gleisner et al. 1996; Boberg et al. 2000; Gleisner and Lundstedt 2001; Karayiannis and Venetsanopoulos 2013). The use of the ANNm application has been common in recent decades, owing to its distinctive features such as learning capability, adaptation to changes, and ease of tools.

Investigations of earth–sun interaction, geomagnetic activities (Gleisner et al. 1996; Boberg et al. 2000; Gleisner and Lundstedt 2001), weather estimations, etc. with ANNs (Gardner and Dorling 1998; Lundstedt et al. 2005; Pallocchia et al. 2006) are effective in terms of space costs-times. ANN models founded by inferring geomagnetic storms' CMEs (Uwamahoro et al., 2012; Singh and Singh 2016) give reasonable results with a high forecasting

ratio of storms. Long-term time data ANN models involving SWp not only forecast the Dst index (Lundstedt, 1992; Lundstedt and Wintoft 1994; Gleisner et al. 1996; Fenrich and Luhman 1998; O'Brien and McPherron 2000; Lundstedt et al. 2002; Bala 2012; Uwamahoro 2012; Singh and Singh 2016) but also estimate geomagnetic activity phases (Gleisner et al., 1996). One may see the difficulty of estimating the Dst index without high-capacity computers with an 84% accuracy. In the 1990s, such an amazing estimation guided the new ANN models (Gleisner et al., 1996). Another ZG indicator Kp index is estimated by the SWp parameters as the proton density (N), the flux velocity (v), and the B_z magnetic field. The Kp index ANN model displays a remarkable estimation ratio (Boberg et al. 2000; Lundstedt 1992). The ap index significant model also utilizes the SWp as proton density and magnetic field (Altadill et al. 2001). The auroral electrojet index AE model uses the proton density (N), the flux density (v), and the magnetic field (B). One may realize from the ANN model estimation more than 70% of the monitored the AE index (Gleisner and Lundstedt, 2001).

This paper investigates different moderate storms separately. Governing the ANN model by the SWp, the ZGi shapes the investigation. In the examination of the first four moderate storms, the correlation matrix specifies the binary relation of the variables, and the dendrogram illustrates the hierarchical cluster of the data. The events that are visualized with graphics are exhibited to the reader. The SW scattering time from bow shock to magnetosphere-ionosphere is not considered in the study when the ZGi from ground stations is utilized.

After the literature review in the "Introduction," yearly ZGi values appearances are seen in "Data" besides variables 5-day scattering. In "Modeling," the ANN model and some properties of data are discussed. The paper is completed with a discussion in "Conclusion."

Data

SPEDAS is used in this essay. Before launching the first four moderate storms of the year 2015 (day by day), one needs a glance at the annual ZGi values. One can find the observed and estimated values of the year 2015 in Fig. 1 besides their absolute errors. The estimated ZGi with the average error variance is as follows:

	Error	Variance
Dst (nT)	0.399 (2.77%)	0.953
ap (nT)	0.271 (2.20%)	0.272
AE (nT)	0.303 (0.14%)	0.243

Fig. 1 Annual observed-estimated Dst (nT) index, ap (nT) index, and AE (nT) index for the year 2015 and their errors
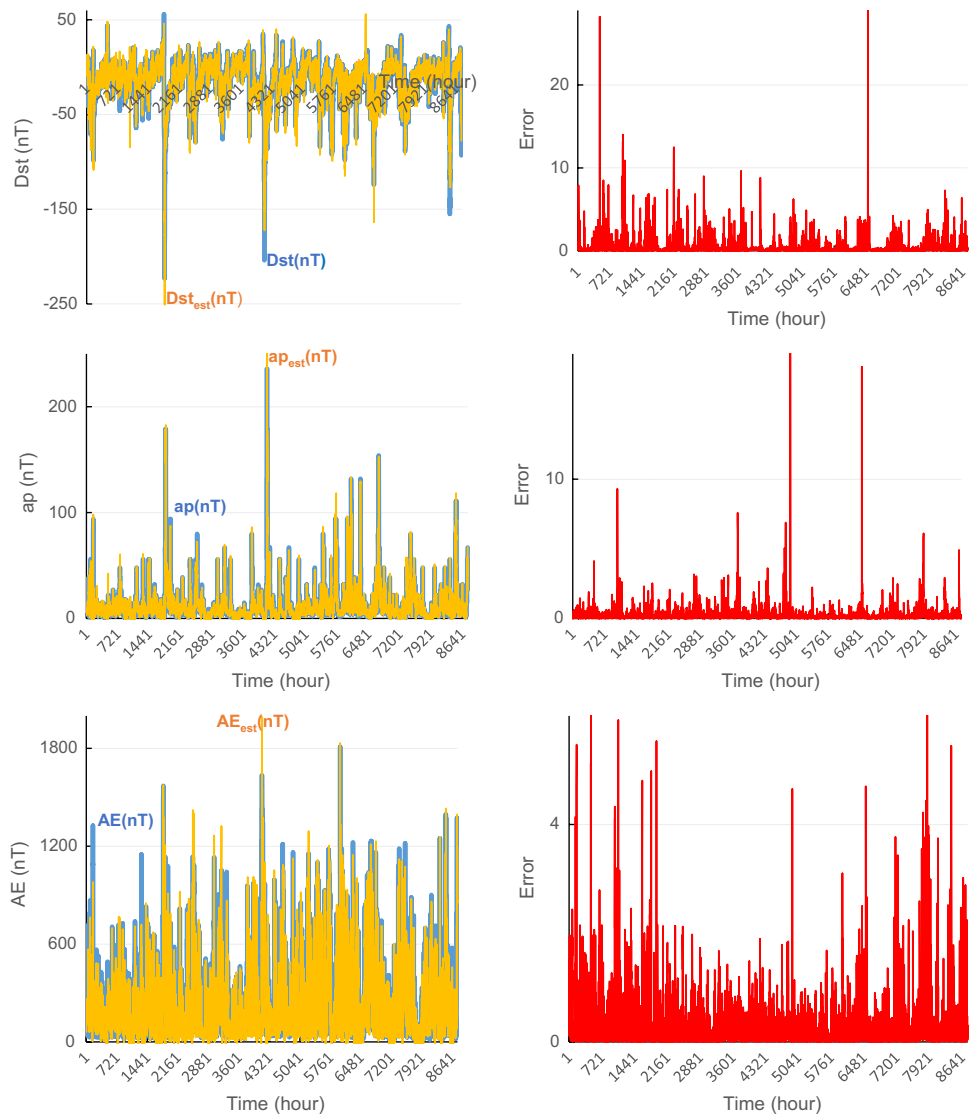
Geomagnetic storms are classified according to the strength of the Dst index (Loewe and Prölss 1997). A Dst index between −50 nT and −30 nT indicates a weak storm, between −100 nT and −50 nT indicates a moderate storm, and between −200 nT and −100 nT indicates a strong (intense, severe) storm. Figure 2 is a 120-h view of some data related to the activities. The storm day is placed in the middle of the 5 days.

It would be appropriate to briefly discuss Fig. 2.

04 January 2015 storm: On 04 January at 14:00 UT, when the B_z magnetic field is at its minimum value of −8.8 nT, the Dst orients to −56 nT and the electric field E shows its maximum value of 3.53 mV/m. Simultaneously, the proton density N indicates to 6.9/cm³, the plasma flow speed v shows 401 km/s, and the pressure P reaches 2.63 nPa. As a response after 2 h, at 16:00 UT, the Dst index and the auroral electrojet AE index hit the minimum–maximum peak values −71 nT and 866 nT, respectively.

On 03 January at 00:00 UT, when the first CME bursts out to the interplanetary medium, instant instability of the dynamic pressure P reaches its peak value of 8.36 nPa with the proton density N, indicating the maximum value of 33.0 1/cm³ and the flow speed v minimum value of 379 km/s.

07 January 2015 storm: After the diminishing in the flow speed v, the first CME hits with the sudden commencement (acceleration) in the dynamic pressure P and the proton density N at 16:00 UT on 06 January. On 07 January at 07:00 UT, the Dst index indicates its peak value of −99 nT, the last CME bursts out. Meantime, the dynamic pressure P jumps from 6.05 nPa to its highest value of 12.36 nPa, and the proton density N hits its maximum value of 29.4 1/cm³. After 2 h, on 07 January at 9:00 UT, the B_z magnetic field decreases to its minimum value (−17.04 nT), the electric field E reaches its highest value of 8.16 mV/m, the AE index shows its maximum value of 1327 nT, and the ap ZG index hits its maximum value of 94 nT.
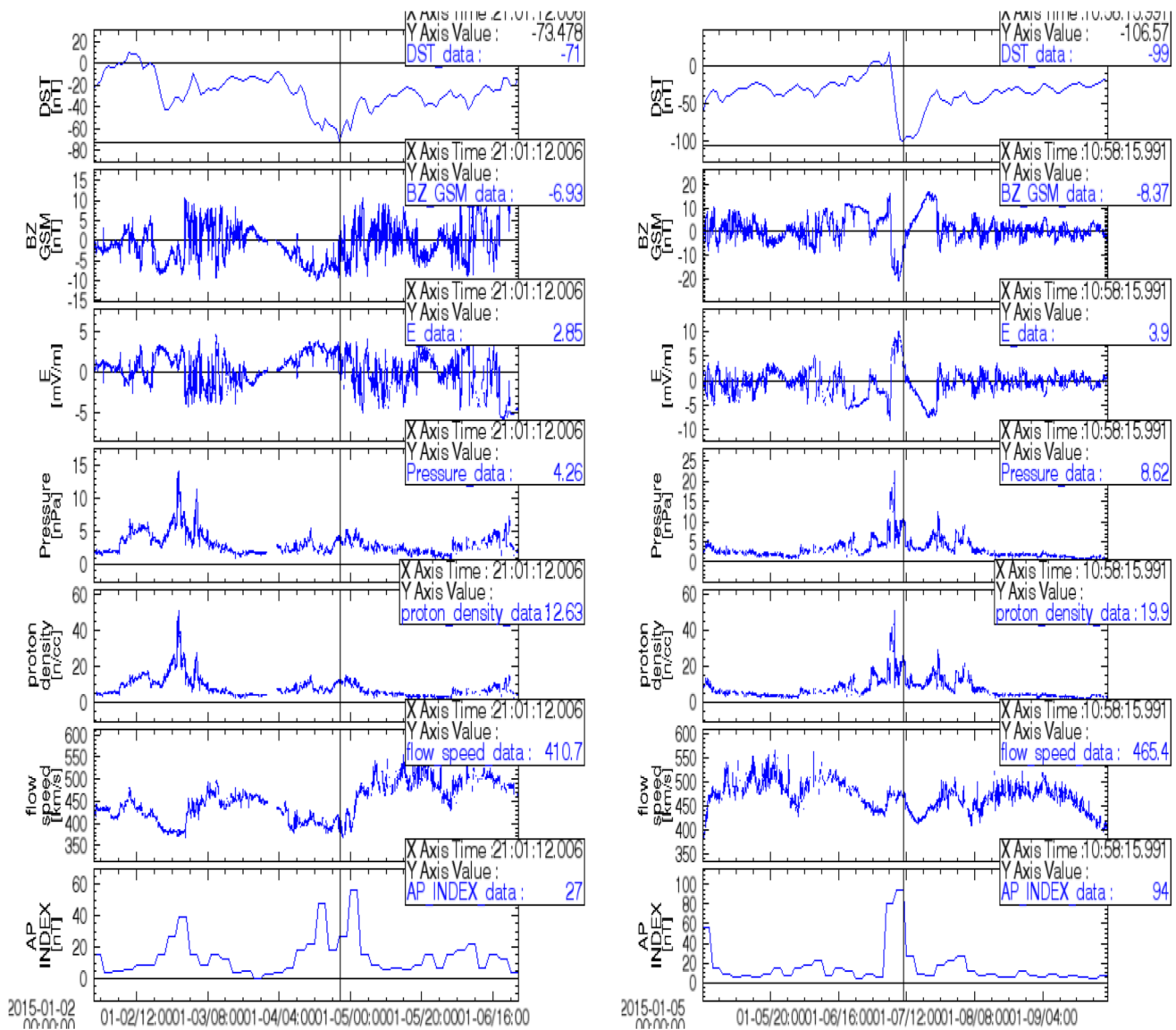
Fig. 2 Data from top to bottom the Dst (nT) index, the Bz magnetic field (nT), the E electric field (mV/m), the dynamic pressure P (nPa), the proton density N (1/cm3), the flow speed v (km/s), and the ap (nT) index for 2015 January 02–06 (upper left side), January 05–09 (upper right side), February 15–19 (bottom left side), and February 22–26 (bottom right side)

17 February 2015 storm: In the 5 days discussion period, when the first CME bursts out on 15 February at 04:00 UT with the sudden commencement in the dynamic pressure P, the proton density N peaks immediately its maximum value of 21.9 $1/cm^3$. On 17 February at 21:00 UT, 3 h before the Dst ZG index takes its minimum value of -62 nT, the magnetic field B_z component indicates its peak value of -12.0 nT and the electric field (E) hits its maximum value of 4.54 mV/m. After 3 h, at 00:00 UT, the ap index, the AE index, and the Dst index indicate their peak values of 48 nT, 579 nT, and -64 nT, respectively.

24 February 2015 storm: In the 5 days storm period, when the first CME bursts out on 23 February at 03:00 UT with the sudden commencement in the dynamic pressure P, the proton density N immediately hits the value of 20.3 $1/cm^3$. After 8 h at 08:00 UT, when the second CME bursts out, the dynamic pressure (P) hits 5.46 nPa and the proton density (N) indicates 20.0 $1/cm^3$. Within 4 h, the magnetic field B_z component hits its peak value of -7.7 nT (11:00 UT), the dynamic pressure (P) increases its maximum value of 8.81 nPa (12:00 UT), and the proton density (N) shows its peak value of 31.7 $1/cm^3$ (at 12:00 UT).
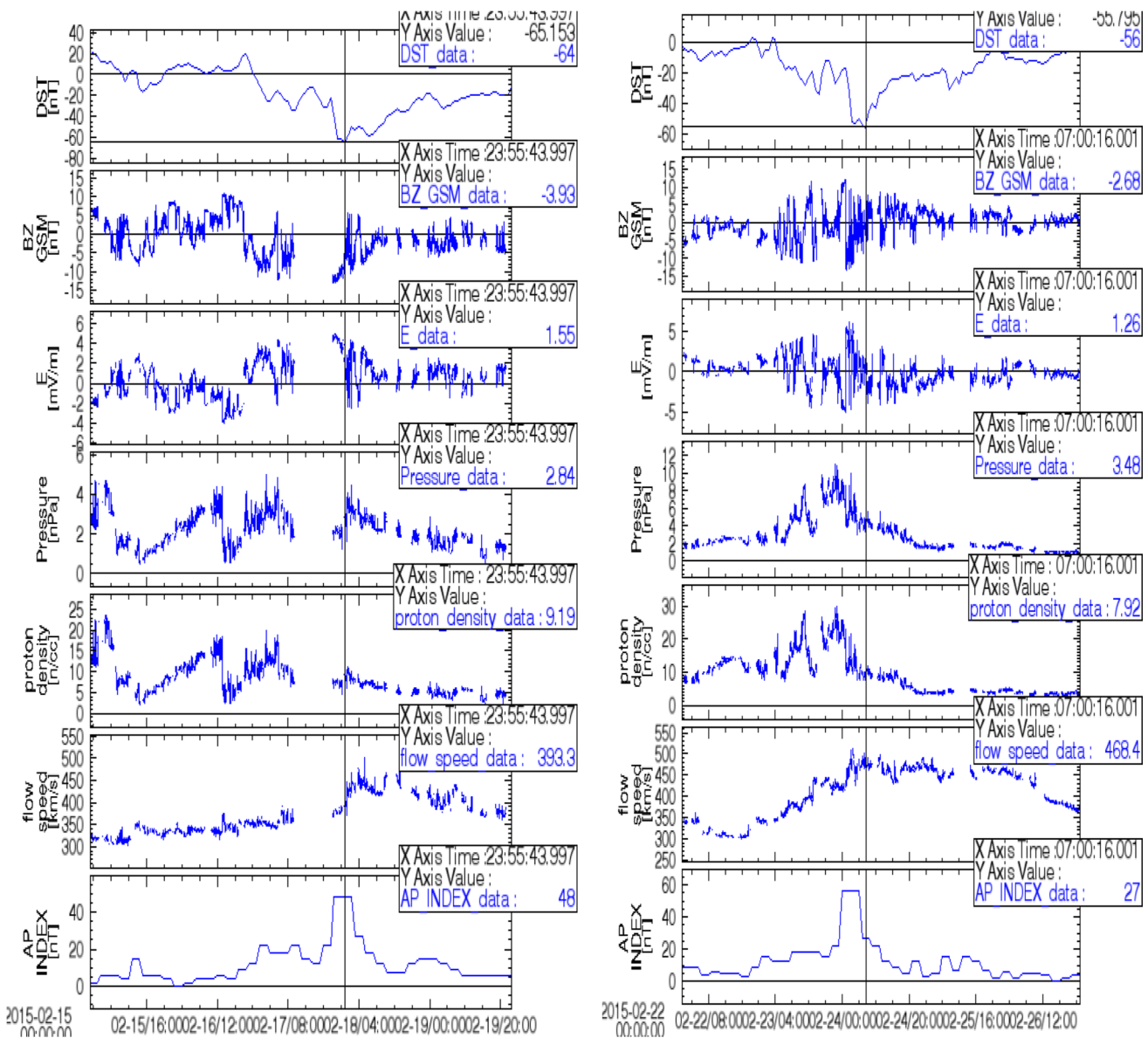
Fig. 2 (continued)

Modeling

Table 1a and 1b demonstrates the binary relationships with the correlation matrix for the data of four moderate storms. The Pearson correlation matrix shows the relationship of variables. When the constants in the matrix are close to ± 1, mutual correlation strengthens. The correlation of the dynamic pressure P and the proton density N parameters in Table 1a and 1b seem high. The reliability of these values can be evaluated with the Cronbach's alpha constant that should be above 60% for reliability. It is 0.645, 0.816, 0.629, and 0.640 in these tables, respectively. Dendrogram of the variables of the storms and scattering of data are specified in Fig. 3a, b and Fig. 4, respectively.

The dendrogram displays the relationship of the variables by each line.

Figure 3a and b shows the dendrogram of the variables of the four moderate storms.

After the introductory mathematical discussion, it can be appropriate to remember the frame of the model of an ANN. The ANNs have been inspired by the working principles of the human brain. This complicated and trainable neural system, which is shaped by linking many neurons with several interface levels, imitates the brain. Studies firstly involved the mathematical modeling of the neurons in the human brain. With increasing awareness, the ANN has become a scientific discipline today with usage areas in many different fields. ANNs can observe information and data in different

Table 1 Correlation of data

04 January 2015

	B_z	T	N	v	P	E	Dst	ap	AE
B_z (nT)	1	0.230*	−0.246**	0.492**	−0.134	−0.996**	0.346**	−0.331**	−0.669**
T (K)		1	−0.263**	0.596**	−0.083	−0.205*	−0.242**	−0.009	−0.145
N (1/cm³)			1	−0.568**	0.932**	0.221*	−0.042	0.426**	0.349**
v (km/s)				1	−0.366**	−0.452**	0.089	−0.344**	−0.424**
P (nPa)					1	0.119	−0.021	0.395**	0.298**
E (mV/m)						1	−0.319**	0.308**	0.635**
Dst (nT)							1	−0.618**	−0.654**
ap (nT)								1	0.628**
AE (nT)									1

07 January 2015

	B_z	T	N	v	P	E	Dst	ap	AE
B_z (nT)	1	0.165	−0.081	−0.150	−0.116	−0.999**	0.122	−0.412**	−0.577**
T (K)		1	−0.417**	0.508**	−0.321**	0.149	0.057	−0.238**	−0.080
N (1/cm³)			1	−0.244**	0.986**	0.091	−0.085	0.657**	0.297**
v (km/s)				1	−0.108	0.136	0.162	−0.066	0.100
P (nPa)					1	0.123	−0.063	0.657**	0.311**
E (mV/m)						1	−0.138	0.415**	0.585**
Dst (nT)							1	−0.291**	−0.540**
ap (nT)								1	0.701**
AE (nT)									1

17 February 2015

	B_z	T	N	v	P	E	Dst	ap	AE
B_z (nT)	1	0.326**	0.027	−0.201*	−0.120	−0.997**	0.522**	−0.513**	−0.630**
T (K)		1	0.307**	0.389**	0.656**	0.326**	−0.439**	0.590**	0.516**
N (1/cm³)			1	−0.431**	0.826**	−0.036	0.342**	0.110	0.031
v (km/s)				1	0.118	0.216*	−0.762**	0.376**	0.346**
P (nPa)					1	0.117	−0.122	0.415**	0.283**
E (mV/m)						1	−0.532**	0.525**	0.628**
Dst (nT)							1	−0.663**	−0.644**
ap (nT)								1	0.648**
AE (nT)									1

24 February 2015

	B_z	T	N	v	P	E	Dst	ap	AE
B_z (nT)	1	0.087	−0.214*	0.370**	−0.057	−0.993**	−0.215*	−0.043	−0.084
T (K)		1	−0.028	0.677**	0.395**	−0.039	−0.779**	0.751**	0.692**
N (1/cm³)			1	−0.414**	0.875**	0.198*	−0.022	0.364**	0.355**
v (km/s)				1	0.038	−0.332**	−0.639**	0.272**	0.239**
P (nPa)					1	0.069	−0.384**	0.605**	0.573**
E (mV/m)						1	0.176	0.075	0.104
Dst (nT)							1	−0.631**	−0.698**
ap (nT)								1	0.743**
AE (nT)									1

**Correlation is significant at the 0.01 level (2-tailed).
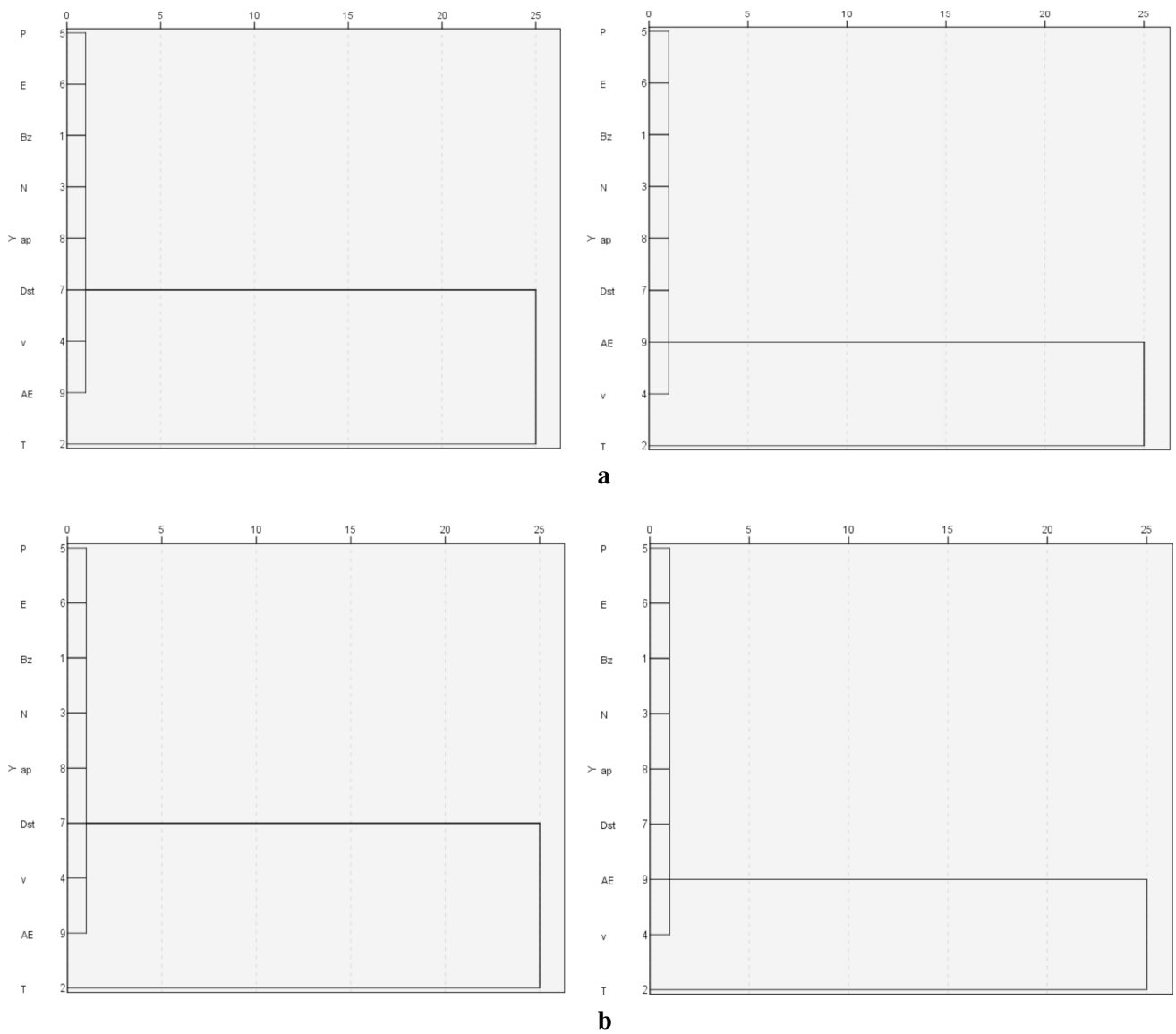*Correlation is significant at the 0.05 level (2-tailed).

Fig. 3 **a** The cluster of the variables (left side: 04 January; right side: 07 January storm); **b** The cluster of the variables (left side: 17 February; right side: 24 February storm)
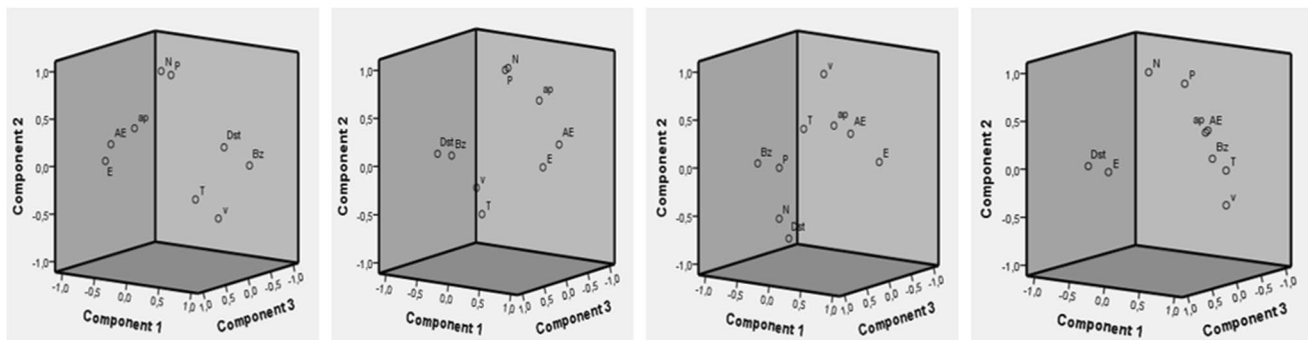

Fig. 4 Scattering of the variables (from left to right: 04 January, 07 January, 17 February, and 24 February storms)

structures and procedures by recognizing them very quickly; they can also reveal unknown and difficult-to-notice correlations among data. They allow modeling without the necessity for any preparation or info among inputs and outputs (Elman 1990). Basically, inputs and corresponding outputs are specified to the network (Fig. 5).

Training or educating of the ANNs requires learning the relationship between input and output. This approach, called instructional learning, is common (Peng et al., 1992). As an architectural configuration involving some layers, the ANN uses data with a pre-determined number of artificial neural cells. The initial layer is generally the *input layer*. This layer is usually not numbered owing to the lack of weight factors and initiation functions of the inputs in the input layer. The second mid-layer, called the *hidden layer*, can be founded so many as needed. Researchers usually employ one hidden layer (Elman 1990; El-Din & Smith 2002). The layer called the *output layer* is the last layer. In this paper, the estimations are completed by the *back propagation* (Rumelhart et al., 1986) ANN algorithm. The typical back propagation algorithm applying a feedback learning structure is the gradient descent algorithm that moves the network weights in the direction of the negative gradient of the performance function. Many backpropagation algorithms appropriate for nearly all problems in ANNs are driven by standard optimization methods such as gradient descent and the Newton approach (Lipmann 1987). Feedback learning using continuous input diminishes the error caused by backward agglomeration. The author utilizes the widely performed Levenberg–Marquardt (trainlm) learning algorithm.

After the creation of the learning algorithm, the number of neurons of the hidden layer has to be specified. The
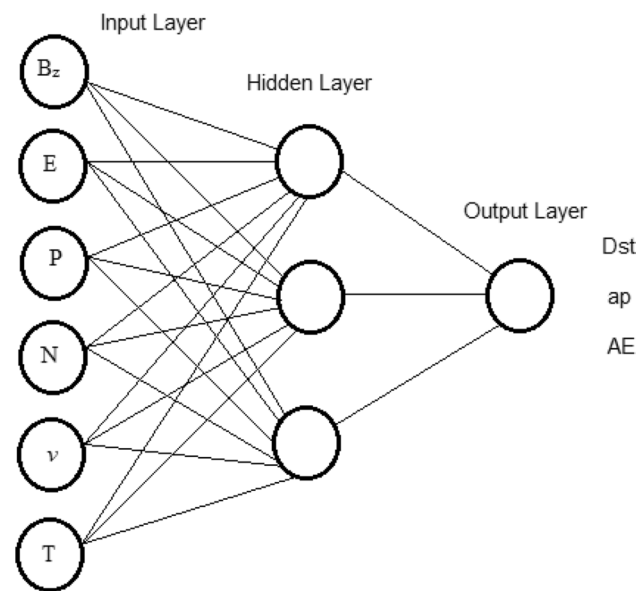
number of neurons should be determined as needed. Too few neurons cause the network to be unable to learn the network pattern, while a large number of neurons cause the network to memorize. A small enough number of neurons forces the ANN to improve the *generalization* facility (Stern 1996). In the paper, the number of neurons in the hidden layer is determined to be thirty-five. In this neuron number, the mean square error (MSE) value begins to indicate no substantial change.

The work consists of three layers: the input layer, hidden layer, and output layer (Fig. 5). In harmony with the causality principle, the SWp (B_z, E, P, N, v, T) are the variables of the input layer and the ZGi (Dst, ap, AE) are the variables of the output layer. For the ANN model to be able to learn well without memorizing, the *sigmoid transfer function* is selected as the neural transition function (Fausett, 1994). A *Linear transfer function* is used in the output layer. Where a total of 120 (5 days) data is investigated, 84 data are utilized for *training* the ANN (70%), 12 data for *validation* (10%) and 24 data for *testing* (20%) (Haykin 1994).

As it may be realized from Fig. 6, the MSE values do not change after 6 updates (step, epoch) for the Dst index, after 8 updates for the ap index, and after 8 updates for the AE index in the 04 January storm (left column). In addition to this, the MSE values do not change after 7 updates for the Dst index, after 8 updates for the ap index, and after 8 updates for the AE index in the 07 January storm (right column). Therefore, learning (training) is finished. Up to these iteration totals, where the best verification performance happens, there is no monitoring of memorization owing to error constancy. Because the validation and test set errors show similar behaviors and no substantial memorization happens, the network performance is acceptable.

One can see from Fig. 6 that MSE values do not change after 7 updates (step, epoch) for the Dst index, after 7 updates for the ap index, and after 6 updates for the AE index in the 17 February storm (left column). In addition to this, the MSE values do not change after 8 updates for the Dst index, after 8 updates for the ap index, and after 8 updates for the AE index in the 24 February storm (right column).

Figure 7a, b and Fig. 8 visualize the results of the discussion. In Fig. 7a and b, the Dst, ap, and AE indices line up from top to bottom, respectively. While Fig. 7a and b displays the correlation, Fig. 8 exhibits the character of observed, forecasted values with their errors. Graphically, forecasting consequences are in Fig. 7a, b between the output and the target (the Dst, ap, AE indices).

Significant studies in the literature have reached remarkable results in the estimation of the Dst, the ap (or the Kp), and the AE index. In the Dst ZG index estimations, Gleisner et al. (1996) achieved an 84% accuracy, Fenrich and Luhman (1998) 79%, O'Brien and McPherron
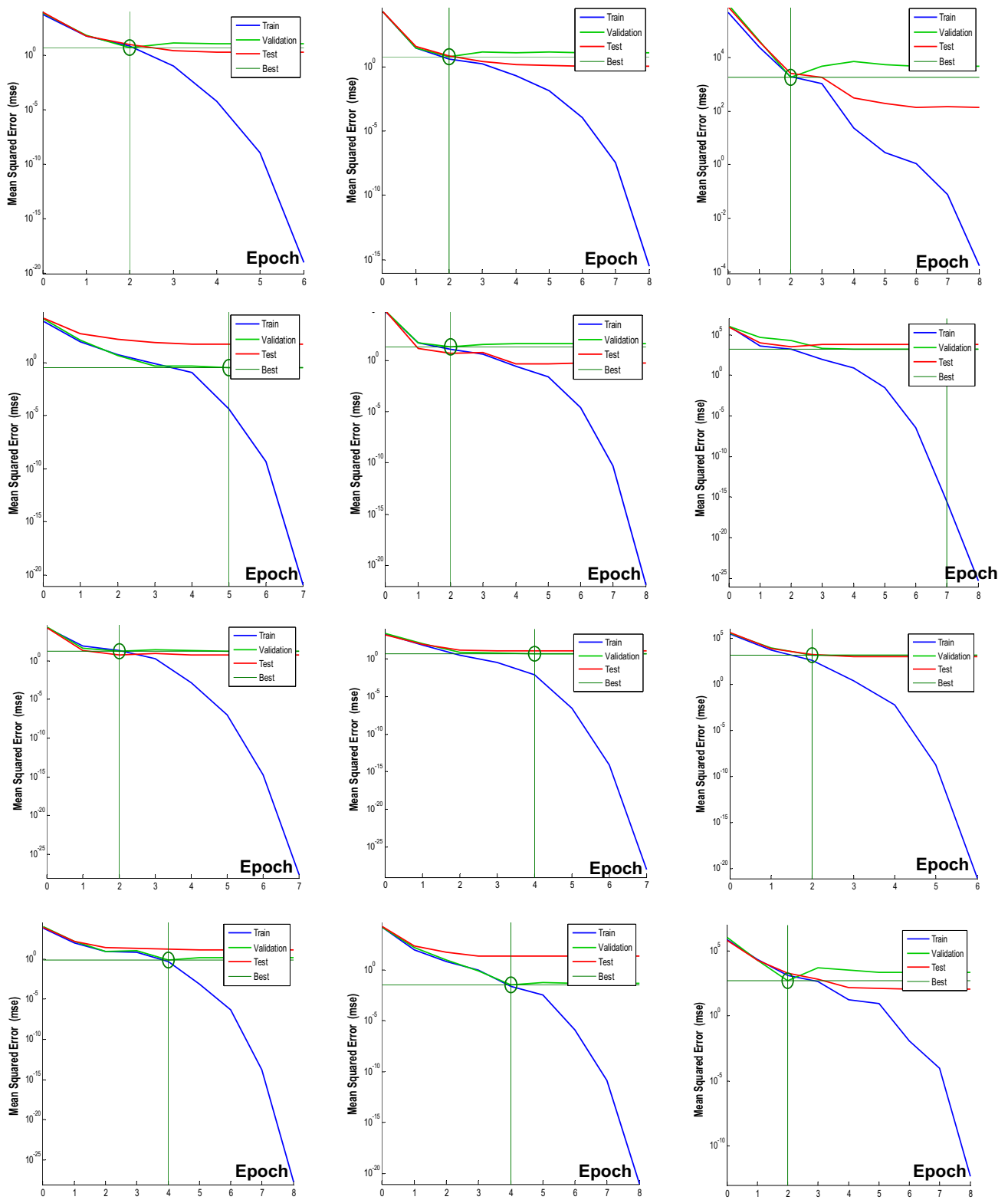
Fig. 5 The ANN framework for the estimation of ZGi

Fig. 6 The chronological performance of the Dst, ap, and AE (from left to right) ANN model
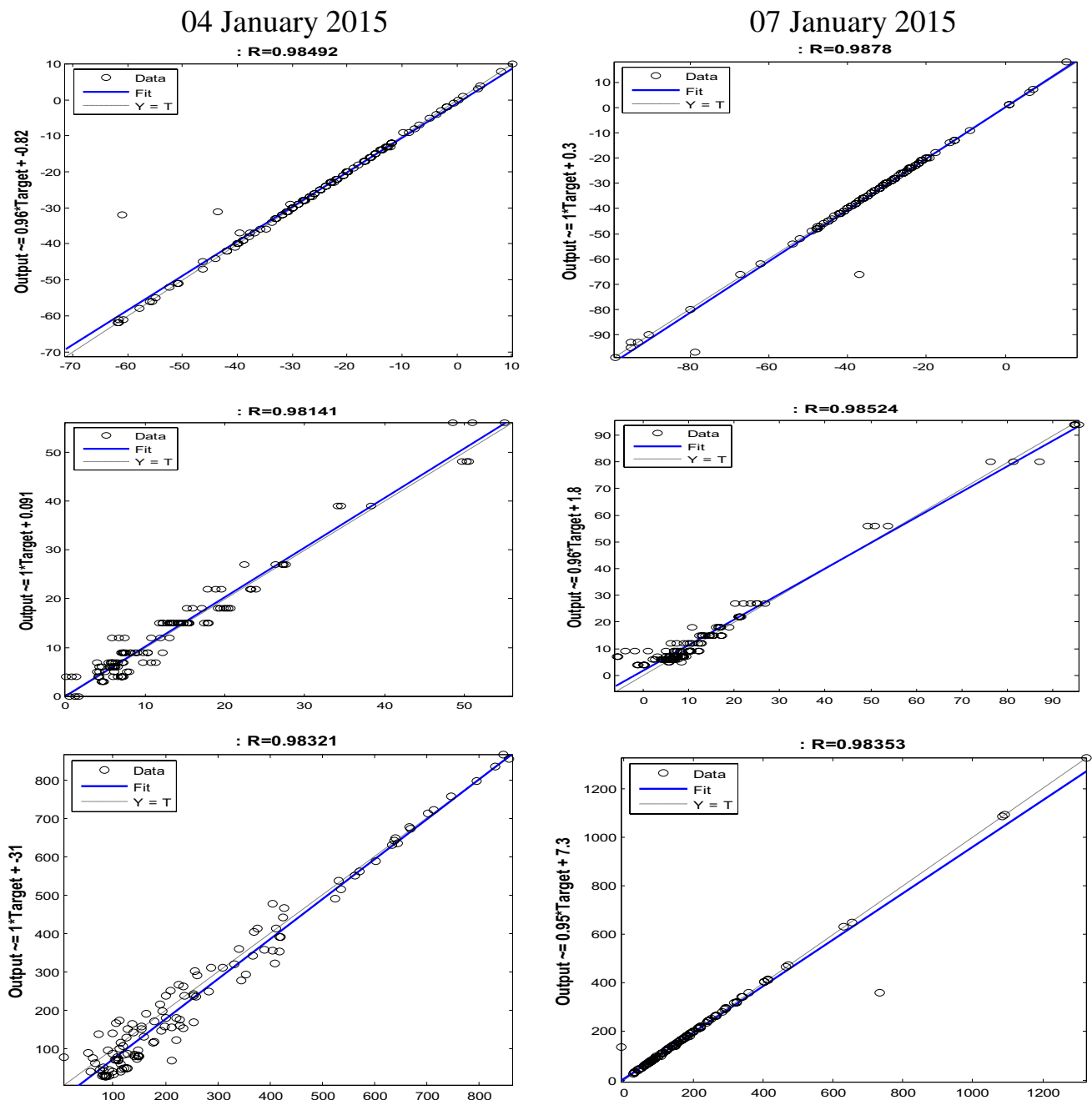
04 January 2015

07 January 2015

Fig. 7 **a** The plot of regression between the estimated and observed Dst, ap, and AE (from top to bottom) indices; **b** The plot of regression between the estimated and observed Dst, ap, and AE (from top to bottom) indices

(2000) 88%, Lundstedt et al. (2002) 88%, Pallocchia et al. (2006) 90%, Bala and Reiff (2012) 86%, Uwamahoro et al. (2012) 86% (for severe storms 100%), Singh and Singh (2016) 79%, and Balan et al. (2017) 100%.

In the Kp ZG index estimations, Boberg et al. (2000) achieved a 77% accuracy, Wing et al. (2005) 94%, Bala and Reiff (2012) 96%, Young et al. (2013) 93%, Solares et al. (2016) 91%, and Wintoft et al. (2017) 92%.

In the AE index estimations, Gleisner et al. (1996) achieved an accuracy of more than 70%, Takalo and Timonen (1997) 98%, Gleisner and Lundstedt (2001) 84%, and Bala and Reiff (2012) 83%.

For the 04 January storm: The Dst, ap, and AE indices estimation models are 98.5%, 98.1%, and 98.3% (Fig. 7a, left column) reliable, respectively.

17 February 2015

24 February2015

Fig. 7 (continued)

For the 07 January storm: The Dst, ap, and AE indices estimation models are 98.8%, 98.5%, and 98.4% (Fig. 7a, right column) reliable, respectively.

For the 17 February storm: The Dst, ap, and AE indices estimation models are 97.6%, 98.9%, and 98.6% (Fig. 7b, left column) reliable, respectively.

For the 24 February storm: The Dst, ap, and AE indices estimation models are 98.9%, 98.5%, and 98.6% (Fig. 7b, right column) reliable, respectively.
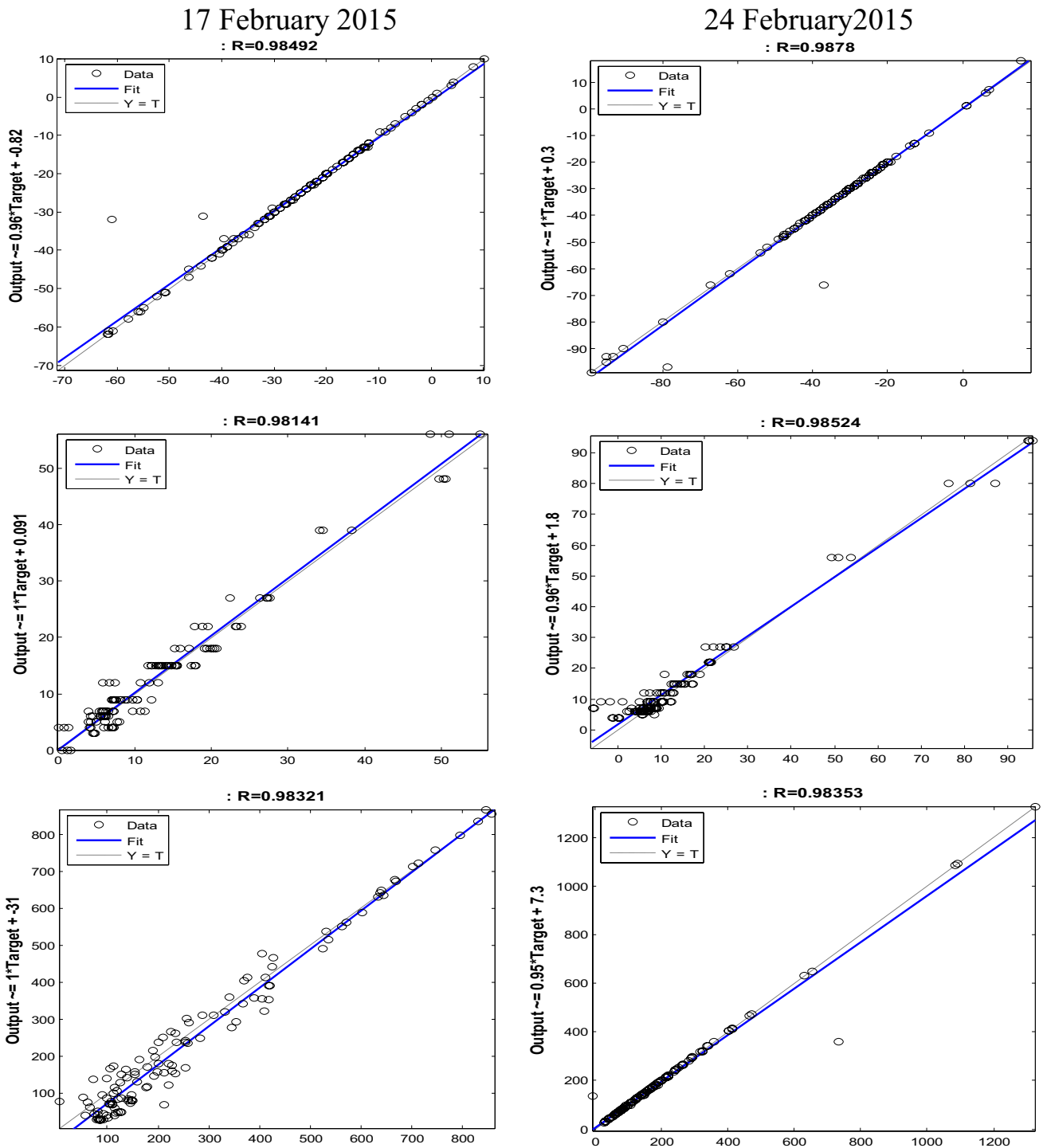
Forecasting model outcomes of the four moderate storms look similar. It is obvious that the ANN model

Fig. 8 The observed and estimated Dst (nT), ap (nT), and AE (nT) indices (chronologically from top to bottom) and their errors

displays the reliable method and the fit output for these moderate geomagnetic activities.

Estimated Dst, ap, and AE indices and their errors for the 04 January moderate storm together with actual ones from NASA are exhibited in Fig. 8, respectively. In Fig. 1 and Fig. 8, one can see the *error* ratio in the comparison of the estimated and monitored Dst, ap, and AE ZGi. The absolute *error* between the real-estimated ZGi values can be observed with the $Error = \left| \frac{Dst_{est} - Dst}{Dst} \right|$, $Error = \frac{|ap_{est} - ap|}{ap}$, and $Error = \frac{|AE_{est} - AE|}{AE}$, where the Dst_{est}, ap_{est}, and AE_{est} are the estimated Dst, ap, and AE index values, respectively. The low error rate exhibits the accuracy of the estimation.

According to Fig. 8, the estimated Dst index average errors are 0.034, 0.009, 0.389, and 0.064 with 0.011, 0.002, 0.841, and 0.012 relative variance values, respectively.

Estimated ap index values and their errors for all storms together with actual ones from NASA are exhibited in Fig. 8, respectively.

According to Fig. 8, the estimated ap index average errors are 0.198, 0.265, 0.035, and 0.019 with 0.047, 0.143, 0.003, and 0.001 their relative variance values, respectively.

Estimated AE index values and their errors for all storms together with actual ones from NASA are displayed in Fig. 8, respectively.

According to Fig. 8, the estimated AE index average errors are 0.444, 0.022, 0.219, and 0.215 with values 0.340, 0.018, 0.111, and 0.056 relative variance values, respectively.

The effect of variables (for solar wind parameters) on the ANN model (Gontarski et al., 2000) can be calculated with the formula % **Effect = 100.(1 − R_n/R_{dif})** by omitting these variables from the investigation process. The correlation coefficients govern this formula. In the formula, R_n is the correlation coefficient attained by excluding the input and R_{dif} is the basic correlation coefficient between estimated and observed values. Table 2a and 2b exhibits the effect of variables on the ANN model.

04 January storm: In the modeling of the Dst (nT) index estimation, the plasma flow speed v (km/s) indicates the main effect. The correlation coefficient diminishes by 13.70% when neglecting the plasma flow speed (Table 2a). The second-high effect belongs to the proton density N (1/cm³) and dynamic pressure P (nPa). The correlation coefficient weakens by 10.37% and 9.43% when omitting the

Table 2 Effect of each variable on the performance of the ANN estimation

Variable	04 January storm						07 January storm					
	Dst (nT)		ap (nT)		AE (nT)		Dst (nT)		ap (nT)		AE (nT)	
	R	Effect on R (%)	R	Effect on R (%)	R	Effect on R (%)	R	Effect on R (%)	R	Effect on R (%)	R	Effect on R (%)
Basic value	**0.985**	-	**0.981**	-	**0.983**	-	**0.988**	-	**0.985**	-	**0.984**	-
B_z (nT)	0.950	3.54	0.838	14.66	0.864	12.16	0.889	10.02	0.885	10.25	0.888	9.76
T (K)	0.982	0.21	0.977	0.71	0.982	0.11	0.980	0.81	0.966	1.92	0.982	0.20
N (1/cm^3)	0.910	10.37	0.899	8.40	0.938	4.60	0.901	8.81	0.814	17.32	0.855	13.11
v (km/s)	0.850	13.70	0.894	8.91	0.915	6.94	0.885	10.53	0.827	16.04	0.890	9.55
P (nPa)	0.892	9.43	0.857	12.64	0.967	1.63	0.866	12.35	0.886	10.05	0.982	0.20
E (mV/m)	0.982	0.20	0.968	1.33	0.968	1.53	0.979	0.91	0.981	0.41	0.973	1.12

Variable	17 February storm						24 February storm					
	Dst (nT)		ap (nT)		AE (nT)		Dst (nT)		ap (nT)		AE (nT)	
	R	Effect on R (%)	R	Effect on R (%)	R	Effect on R (%)	R	Effect on R (%)	R	Effect on R (%)	R	Effect on R (%)
Basic value	**0.976**	-	**0.989**	-	**0.986**	-	**0.989**	-	**0.985**	-	**0.986**	-
B_z (nT)	0.909	6.86	0.889	10.11	0.913	7.40	0.758	23.36	0.906	8.02	0.915	7.20
T (K)	0.971	0.51	0.978	1.11	0.982	0.41	0.980	0.91	0.983	0.20	0.983	0.21
N (1/cm^3)	0.903	7.48	0.883	10.72	0.919	6.80	0.908	8.19	0.807	18.10	0.871	11.66
v (km/s)	0.896	8.20	0.900	9.00	0.909	7.73	0.909	8.03	0.861	12.59	0.916	7.10
P (nPa)	0.907	7.07	0.892	9.81	0.980	0.61	0.860	13.04	0.912	7.41	0.982	0.41
E (mV/m)	0.971	0.51	0.969	2.02	0.971	1.52	0.986	0.30	0.964	2.23	0.984	0.20

proton density and dynamic pressure P value, respectively (Table 2a). Finally, when omitting the magnetic field B_z (nT) component, the Dst index is affected by 3.54%. The plasma flow speed v (km/s), the proton density N (1/cm^3), the dynamic pressure P (nPa), and the magnetic field B_z (nT) are indispensable estimators for the Dst (nT) index (Burton et al. 1975; Gleisner et al. 1996). Physically, coronal holes created by the instability of hot particles are the origin of the flow speed v (km/s). The SW streams have high speed. The polarization of the magnetic field is indicated by the parameters of the SW speed (Tsurutani et al., 2006). Besides orienting the magnetic field B_z (nT) component from southward to northward and indicating its negative values, the flow speed v (km/s) shapes the geomagnetic storm. The flow speed v (km/s) and the B_z (nT) component, with these anomalous replies, show that the Dst (nT) index should decline to a negative minimum. By enhancing the proton density N (1/cm^3), the high-density plasma dynamic pressure P (nPa) and SW suppress the magnetosphere (Tsurutani et al., 2006). The reflection of the disturbance caused by this compress governed by the flow speed v (km/s) is the Dst (nT) index. Accordingly, one of the principal motivations why the Dst (nT) index decreases to minimum value is the flow speed (Gonzalez et al. 1989; Borovsky 2012; Borovsky and Yakymenko 2017). The ANN model shapes the estimation of the Dst values with the literature (Table 2a and 2b).

The maximum impact on the ap (nT) index estimation takes into account the magnetic field B_z (nT) component, the dynamic pressure P (nPa), the flow speed v (km/s), and proton density N (1/cm^3). When the magnetic field and the dynamic pressure are omitted, the correlation ratio declines by 14.66% and 12.64%, respectively (Table 2a). The flow speed v (km/s) and the proton density N (1/cm^3) are also other high parameters for the ap index. If these variables are omitted from the ap estimation, the model correlation constant diminishes by 8.91% and 8.40%, respectively. Physically, magnetic field polarizations indicate parallel effects with the dynamic pressure P (nPa), the flow speed v (km/s), and the proton density N (1/cm^3), while the ap index nonlinearly responses to the instabilities (Altadill et al. 2001; Eroglu 2018; 2019, 2020, 2021; Inyurt 2020; Koklu 2020). The noticeable relation between the B_z (nT) magnetic field, the dynamic pressure P (nPa), the flow speed v (km/s), the proton density N (1/cm^3), and the ap (nT) index may be seen in Table 2a.

In the ANN estimation model for the AE (nT) index, the highest impact relates to the magnetic field B_z (nT) component. One may see that when neglecting the B_z (nT) magnetic field, the correlation constant decreases by 12.16% (Table 2a). The magnetic field is accompanied by the flow speed v (km/s) and proton density N (1/cm^3) during the calculation of the AE (nT) index correlation ratio. It is realized that the value of R declines by 6.94% and 4.60% when the

flow speed v (km/s) and proton density N (1/cm^3) are subtracted from the ANN model of the AE index, respectively (Table 2a) (Gleisner and Lundstedt, 2001).

07 January storm: Parallel conclusions can also be drawn for the 07 January moderate storm. In the Dst index estimation, the highest effect belongs to the dynamic pressure P (nPa), the flow speed v (km/s), and the B_z (nT) magnetic field. The correlation coefficient diminishes by 12.35%, 10.53%, and 10.02% when neglecting the mentioned SWp value, respectively (Table 2a). According to Table 2a, the proton density N (1/cm^3) affects the Dst (nT) index with a value of 8.81%.

The maximum impact on the ap (nT) index estimation takes into account the proton density N (1/cm^3) and the flow speed v (km/s). When the proton density and the flow speed are omitted, the correlation constant value decreases by 17.32% and 16.04%, respectively (Table 2a). Secondly, the other main factors are the B_z magnetic field (nT) and the dynamic pressure P (nPa) for the ap (nT) index. If they are omitted from the ap (nT) prediction, the model correlation ratio decreases by 10.25% and 10.05%, respectively (Table 2a).

In the estimation of the AE (nT) index, the highest effect belongs to the proton density N (1/cm^3). One can see that when neglecting the proton density, the correlation constant value decreases by 13.11% (Table 2a). Besides the proton density, it is observed that the value of R decreases by 9.76% and 9.55% when the magnetic field B_z (nT) component and the flow speed v (km/s) are excluded from the AE index model, respectively (Table 2a).

17 February storm: This moderate storm also reflects similar effects. The Dst (nT) index estimation responds to ignoring the flow speed v (km/s), the proton density N (1/cm^3), the dynamic pressure P (nPa), and the B_z (nT) magnetic field. The correlation constant decreases by 8.20%, 7.48%, 7.07%, and 6.86% when neglecting mentioned SWp value, respectively (Table 2b).

The maximum effect on the ap (nT) index estimation takes into account the proton density N (1/cm^3), the B_z magnetic field (nT), the dynamic pressure P (nPa), and the flow speed v (km/s). When the mentioned SWp is omitted, the correlation constant value decreases by 10.72%, 10.11%, 9.81%, and 9.00%, respectively (Table 2b).

In the estimation of the AE (nT) index, the highest effect belongs to the flow speed v (km/s), the magnetic field B_z (nT) component, and proton density N (1/cm^3). One can realize that when neglecting these parameters, the correlation constant value decreases by 7.73%, 7.40%, and 6.80%, respectively (Table 2b).

24 February storm: Lastly, according to the 24 February moderate storm, the Dst (nT) index estimation is deeply related to the B_z (nT) magnetic field, the dynamic pressure P (nPa), the proton density N (1/cm^3), and the flow speed v

(km/s). The correlation coefficient diminishes by 23.36%, 13.04%, 8.19%, and 8.03% when neglecting these SWp, respectively (Table 2b).

The maximum impact on the ap (nT) index estimation takes into account the proton density N ($1/cm^3$), the flow speed v (km/s), the B_z magnetic field (nT), and the dynamic pressure P (nPa). When the mentioned SWp is omitted, the correlation constant value decreases by 18.10%, 12.59%, 8.02%, and 7.41%, respectively (Table 2b). Secondly, the electric field E (mV/m) affects the ap (nT) index by 2.23% (Table 2b).

In the estimation of the AE (nT) index, the highest effect is observed by means of the proton density N ($1/cm^3$), the B_z (nT) magnetic field, and the flow speed v (km/s). One can see that when ignoring these SWp, the correlation constant value decreases by 11.66%, 7.20%, and 7.10%, respectively (Table 2b).

Conclusion

The purpose of the study is to assess the four moderate geomagnetic storms that occurred in the year 2015. After glancing at the year 2015 as a whole, zonal geomagnetic indices (ZGi) of these first four moderate activities are estimated efficiently. When comparing the estimation of geomagnetic storms by the artificial neural network (ANN) with the literature, the conclusions are satisfactory.

For these events, it is notable that the ANN model estimates the ZGi considering the solar wind (SWp). A geomagnetic storm strength and its phases may be evaluated by discussing the ZGi. The paper is based on the method of inputting the SWp to the ANN model and yielding the ZGi as the output. The estimation performance of the ANN model with ZGi as the output is acceptable and consistent for the literature. The results demonstrate that the model is over 90% consistent in the estimation of the ZGi of these four moderate storms. The essay, in addition to the estimation, discusses the effect of the SW variables on the ANN model for these storms.

Regarding the proton density (N), the flow speed (v), the magnetic field z component (B_z), the dynamic pressure (P), and the electric field (E), according to the 04 January storm ANN model, for the Dst index, the v, N, and P have a high effect, while the B_z component has the moderate effect. Furthermore, B_z field, P, and v with N affect the ap index highly. For the auroral electrojet index AE, B_z has a high effect, v and N have a moderate effect.

According to the ANN model of the 07 January moderate storm, for the Dst index, P, v, B_z, and N have a high effect. Moreover, N, v, and B_z with P affect the ap index highly. For the AE index, N, B_z field, and v have a high effect.

According to the ANN model of the 17 February storm, for the Dst index, v, N, P, and B_z have a high effect. Additionally, N, B_z, and P with v affect the ap index highly. The electric field (E) also has a moderate effect on the ap ZG index. In calculating auroral electrojet index AE, v, B_z, and N have a high effect.

According to the ANN estimation model of the 24 February moderate storm, for the Dst ZG index, B_z has a very high effect and P, N, and v has a high effect. Furthermore, for the ap ZG index, N has a very high effect and v, B_z field, and P have a high effect besides the moderate effect of E. For the AE index, N, B_z, and v have a high effect.

The agreement between the result of this study and those of previous studies indicates the reliability of the results of this study. The author expects to contribute to geomagnetic storm estimations by making it easier to understand their dynamics. The Dst, ap, and AE indices estimated for these storms can also be estimated for other storms. With a similar approach, it will not be difficult for the ANN model to estimate the ZGi of weak, moderate, or severe storms. The indices considered together with the SWp prepare the ground for predictable storms. The author hopes to attain the same results for weak, moderate, and severe storms in further discussions.

Declarations

Conflict of interest The author declares that he has no competing interests.

References

Akasofu SI (1964) The development of the auroral substorm. Planet Space Sci 12(4):273–282. https://doi.org/10.1016/0032-0633(64)90151-5

Altadill D, Apostolov EM, Sole JG, Jacobi CH (2001) Origin and development of vertical propagating oscillations with periods of planetary waves in the ionospheric F region. Solar Terrestr Planet Sci 26(6):387–393. https://doi.org/10.1016/S1464-1917(01)00019-8

Bala R, Reiff P (2012) Improvements in short-term forecasting of geomagnetic activity. Space Weather 10(6):779. https://doi.org/10.1029/2012SW000779

Balan N, Ebihara Y, Skoug R, Shiokawa K, Batista IS, Tulasi Ram S, Omura Y, Nakamura T, Fok MC (2017) A scheme for forecasting severe space weather. J Geophys Res Space Physics 122(3):2824–2835. https://doi.org/10.1002/2016JA023853

Boberg F, Wintoft P, Lundstedt H (2000) Real time Kp predictions from solar wind data using neural networks. Phys Chem Earth Part C 25(4):275–280. https://doi.org/10.1016/S1464-1917(00)00016-7

Borovsky JE (2012) The velocity and magnetic field fluctuations of the solar wind at 1 AU: statistical analysis of Fourier spectra and

correlations with plasma properties. J Geophys Res Space Physics 117(A5):A05104. https://doi.org/10.1029/2011JA017499

Borovsky JE, Yakymenko K (2017) Systems science of the magnetosphere: creating indices of substorm activity, of the substorm-injected electron population, and of the electron radiation belt. J Geophys Res Space Physics 122(10):10012–10035. https://doi.org/10.1002/2017JA024250

Burton RK, McPherron RL, Russell CT (1975) An empirical relationship between interplanetary conditions and Dst. J Geophys Res 80(31):4204–4214. https://doi.org/10.1029/JA080i031p04204

Conway AJ (1998) Time series, neural networks and the future of the sun. New Astron Rev 42(5):343–394. https://doi.org/10.1016/S1387-6473(98)00041-4

Dungey JW (1961) Interplanetary magnetic field and the auroral zones. Phys Rev Lett 6:47. https://doi.org/10.1103/PhysRevLett.6.47

ElDin AG, Smith DW (2002) A neural network model to predict the wastewater inflow incorporating rainfall events. Water Res 36(5):1115–1126

Elman JL (1990) Finding structure in time. Cogn Sci 14:179

Eroglu E (2018) Mathematical modeling of the moderate storm on 28 February 2008. New Astron 60:33. https://doi.org/10.1016/j.newast.2017.10.002

Eroglu E (2019) Modeling the superstorm in the 24th solar cycle. Earth Planets Spaces 71:26. https://doi.org/10.1186/s40623-019-1002-1

Eroglu E (2020) Modeling of 21 July geomagnetic storm. J Eng Technol Appl Sci 5(1):33. https://doi.org/10.30931/jetas.680416

Eroglu E (2021) Zonal geomagnetic indices estimation of the two super geomagnetic activities of 2015 with the artificial neural networks. Adv Space Res 68(6):2272–2284. https://doi.org/10.1016/j.asr.2021.04.036

Eroglu E, Aksoy S, Tretyakov OA (2012a) Surplus of energy for time-domain waveguide modes. Energy Educ Sci Tech 29(1):495

Eroglu E, Ak N, Koklu K, Ozdemir Z, Celik N, Eren N (2012b) Special functions in transferring of energy; a special case: "Airy function." Energy Educ Sci Tech 30(1):719

Eroglu, E., "Dalga Kılavuzları Boyunca Geçici Sinyallerin Transferi", Ph.D. Thesis, Gebze High Technology Institute, 2011.

Fausett LV (1994) Fundamentals of neural networks: architecture, algorithms and applications. Prentice-Hall Inc, Englewood Cliffs

Fenrich FR, Luhmann JG (1998) Geomagnetic response to magnetic clouds of different polarity. Geophys Res Lett 25(15):2999–3002. https://doi.org/10.1029/98GL51180

Fu HS, Khotyaintsev YuV, Vaivads A, Retinò A, André M (2013) Energetic electron acceleration by unsteady magnetic reconnection. Nat Phys 9:426–430. https://doi.org/10.1038/nphys2664

Fu HS, Vaivads A, Khotyaintsev YV, André M, Cao JB, Olshevsky VJ, Eastwood P, Retinò A (2017) Intermittent energy dissipation by turbulent reconnection. Geophys Res Lett 44(1):37–43. https://doi.org/10.1002/2016GL071787

Gardner MW, Dorling SR (1998) Artificial neural networks (the multilayer perceptron)—a review of applications in the atmospheric sciences. Atmos Environ 32(14–15):2627–2636. https://doi.org/10.1016/S1352-2310(97)00447-0

Gleisner H, Lundstedt H (2001) Auroral electrojet predictions with dynamic neural networks. J Geophys Res Space Physics 106(A11):24541–24549. https://doi.org/10.1029/2001JA900046

Gleisner H, Lundstedt H, Wintoft P (1996) Predicting geomagnetic storms from solar-wind data using time-delay neural networks. Ann Geophys 14:679–866

Gontarski CA, Rodrigues PR, Mori M, Prenem LF (2000) Simulation of an industrial wastewater treatment plant using artificial neural networks. Comput Chem Eng 24(2):1719–1723

Gonzalez WD, Tsurutani BT, Gonzalez ALC, Smith EJ, Tang F, Akasofu SI (1989) Solar wind-magnetosphere coupling during intense magnetic storms (1978–1979). J Geophys Res 94(A7):8835. https://doi.org/10.1029/ja094ia07p08835

Gonzalez WD, Tsurutani BT, Gonzalez AL (1999) Interplanetary origin of geomagnetic storms. Space Sci Rev 88:529–562. https://doi.org/10.1023/A:1005160129098

Haykin S (1994) Neural networks – a comprehensive foundation. Macmillan College Publ. Comp. Inc, New York

Inyurt S (2020) Modeling and comparison of two geomagnetic storms. Adv Space Res 65(3):966. https://doi.org/10.1016/j.asr.2019.11.004

Inyurt S, Sekertekin A (2019) Modeling and predicting seasonal ionospheric variations in Turkey using artificial neural network (ANN). Astrophys Space Sci 364(4):62

Kamide Y, Baumjohann W, Daglis LA, Gonzalez WD, Grande M, Joselyn JA, McPherron RL, Phillips JL, Reeves GD, Rostoker G, Shanna AS, Singer HJ, Tsurutani BT, Vasyliuna VM (1998) Current understanding of magnetic storms' storm-substorm relationships. J Geophys Res 103(A8):17705

Karayiannis N, Venetsanopoulos AN (2013) "Artificial neural networks: learning algorithms, performance evaluation, and applications. Springer Science & Business Media 209:373

Koklu K (2020) Mathematical analysis of the 09 March 2012 intense storm. Adv Space Res 66(4):932. https://doi.org/10.1016/j.asr.2020.04.053

Lin J, Ni L (2018) Electric currents in geospace and beyond, Geophysical Monograph 235, 11th edn. John Wiley & Sons Inc, Hoboken

Lippmann RP (1987) An introduction to computing with neural nets. ASSP Magazine, IEEE 4(2):4–22

Loewe CA, Prölss GW (1997) Classification and mean behavior of magnetic storms. J Geophys Res 102(A7):14209

Lundstedt H (1992) Neural networks and predictions of solar-terrestrial effects. Planet Space Science 40(4):457–464. https://doi.org/10.1016/0032-0633(92)90164-J

Lundstedt H, Wintoft P (1994) Prediction of geomagnetic storms from solar wind data with the use of a neural network. Ann Geophys 12:19–24. https://doi.org/10.1007/s00585-994-0019-2

Lundstedt H, Gleisner H, Wintoft P (2002) Operational forecasts of the geomagnetic Dst index. Geophys Res Lett 29(24):2181. https://doi.org/10.1029/2002GL016151

Lundstedt H, Liszka L, Lundin R (2005) Solar activity explored with new wavelet methods. Ann Geophys 23:1505–1511. https://doi.org/10.5194/angeo-23-1505-2005

Mayaud PN (1980) Derivation, meaning, and use of geomagnetic indices. Geophys Monogr Ser 22:154. https://doi.org/10.1029/GM022

O'Brien TP, McPherron RL (2000) Forecasting the ring current index Dst in real time. J Atmos Solar Terr Phys 62(14):1295–1299. https://doi.org/10.1016/S1364-6826(00)00072-9

Pallocchia G, Amata E, Consolini G, Marcucci MF, Bertello I (2006) Geomagnetic Dst index forecast based on IMF data only. Ann Geophys 24:989–999. https://doi.org/10.5194/angeo-24-989-2006

Parker EN (1958) Dynamics of the interplanetary gas and magnetic fields. Astrophys J 128:664

Peng TM, Hubele NF, Karady GG (1992) Advancement in the application of neural networks for STLF. IEEE Trans Power Syst 7(1):250–257

Rathore B, Gupta D, Parashar K (2014) Relation between solar wind parameter and geomagnetic storm condition during Cycle-23. Int J Geosci 5(13):513131. https://doi.org/10.4236/ijg.2014.513131

Rumelhart DE, Hinton GE, Williams RJ (1986) Learning representations by back-propagating errors. Nature 323:533–536

Singh G, Singh AK (2016) A study on precursors leading to geomagnetic storms using artificial neural network. J Earth Syst Sci 125:899–908. https://doi.org/10.1007/s12040-016-0702-1

Solares JRA, Wei HL, Boynton RJ, Walker SN, Billings SA (2016) Modeling and prediction of global magnetic disturbance in near-Earth space: a case study for Kp index using NARX models. Space Weather 14(10):899–916. https://doi.org/10.1002/2016SW001463

Stern HS (1996) Neural networks in applied statistics. Technometrics 38(3):205–214

Sugiura M (1964) Hourly values of the equatorial Dst for IGY. Annals of the International Geophysical Year, vol 35. Pergamon Press, Oxford, pp 945–948

Takalo J, Timonen J (1997) Neural network prediction of AE data. Geophys Res Lett 24:2403–2406. https://doi.org/10.1029/97GL02457

Tsurutani BT, Gonzalez WD, Gonzalez ALC, Guarnieri FL, Gopalswamy N, Grande M, Kamide Y, Kasahara Y, Lu G, Mann I, Mcpherron R, Soraas F, Vasyliunas V (2006) Corotating solar wind streams and recurrent geomagnetic activity: a review. J Geophys Res Space Phys 111(A7):11273. https://doi.org/10.1029/2005JA011273

Uwamahoro J, McKinnell LA, Habarulema JB (2012) Estimating the geoeffectiveness of halo CMEs from associated solar and IP parameters using neural networks. Ann Geophys 30:963–972. https://doi.org/10.5194/angeo-30-963-2012

Williams RJ, Zipser D (1989) A learning algorithm for continually running fully recurrent neural networks. Neural Comput 1(2):270–280. https://doi.org/10.1162/neco.1989.1.2.270

Wing S, Johnson JR, Jen J, Meng CI, Sibeck DG, Bechtold K, Freeman J, Costello K, Balikhin M, Takahashi K (2005) Kp forecast models. J Geophys Res Space Phys 110(A4). https://doi.org/10.1029/2004JA010500

Wintoft P, Wik M, Matzka J, Shprits Y (2017) Forecasting Kp from solar wind data: input parameter study using 3-hour averages and 3-hour range values. J Space Weather Space Clim 7:A29. https://doi.org/10.1051/swsc/2017027

Young EJ, Moon YJ, Park J, Lee JY, Lee DH (2013) Comparison of neural network and support vector machine methods for Kp forecasting. JGR Space Physics 118(8):5109–5117